JOURNAL OF AGRICULTURAL AND FOOD CHEMISTRY

The Physics and Chemistry behind the Bubbling Properties of Champagne and Sparkling Wines: A State-of-the-Art Review

GÉRARD LIGER-BELAIR†

Laboratoire d'Œnologie et de Chimie Appliquée, UPRES EA 2069, Université de Reims Champagne-Ardenne, B.P. 1039, 51687 Reims Cedex 2, France

In this review, the latest results about the chemical physics behind the bubbling properties of Champagne and sparkling wines are collected and fully illustrated. The chemistry of carbon dioxide molecules dissolved into the liquid matrix (section 2) is presented, as are the three main steps of a fleeting bubble's life, that is, the bubble nucleation on tiny particles stuck on the glass wall (section 3), the bubble ascent and growth through the liquid matrix (section 4), and the bursting of bubbles at the liquid surface (section 5), which constitutes the most intriguing, functional, and visually appealing step.

Keywords: Champagne; sparkling wines; beer; carbonated beverages; carbon dioxide; effervescence; bubbles; bubbling properties

1. INTRODUCTION

Effervescence (from the Latin *fervere*: to boil), which is related to gas discharching from a liquid by bubbling, is the main characteristic of Champagne and sparkling wines. Careful observation of a glass poured with Champagne shows bubble trains rising gracefully toward the liquid surface. Since the time of the Benedictine monk Dom Pierre Perignon (1638−1715), Champagne has been the wine of celebration (*1*, *2*). This fame is largely linked to the elegance of its effervescence and foaming properties. The quality of the product is often related to the size of bubbles formed in the flute. Small bubbles rising slowly through the liquid are much preferred to large bubbles. Bubbles formed in the glass are also responsible for the aspect of the foam ring on the liquid surface, the so-called *collerette*, which is also an important feature of this product. But, even if there is no evidence yet to believe that bubbles confer any other sensory advantage to the wine, it is often recognized that bubbles play a major role in the assessment of a Champagne wine. Bubble size may also have an effect on flavor release and mouthfeel.

In light of this, it is important to better detect, understand, and study the various parameters involved in this phenomenon. This review collects the latest results about the bubbling properties of Champagne and sparkling wines obtained during the past few years.

2. CHAMPAGNE: A LIQUID SUPERSATURATED WITH CO_2 MOLECULES

2.1. Before Uncorking the Bottle. The main gas responsible for effervescence in Champagne and sparkling wines is carbon dioxide (CO_2), which is produced in closed bottles during the second alcoholic fermentation or "prise de mousse". CO_2 molecules form together with ethanol when yeast ferment sugars, according to the following equation discovered by the French chemist and microbiologist Louis Pasteur in the mid 19th century.

$$C_6H_{12}O_6 \rightarrow 2CH_3CH_2OH + 2CO_2 \quad (1)$$

Actually, the bottles are sealed, so that the CO_2 molecules cannot escape and progressively dissolve into the wine. During this second, slow fermentation process, the carbon dioxide dissolved in the wine and the gaseous carbon dioxide under the cork progressively establish equilibrium—an application of Henry's law, which states that the partial pressure of a given gas above a solution is proportional to the concentration of the gas dissolved into the solution, as expressed by the relationship

$$c = k_H P_{CO_2} \quad (2)$$

where c is the concentration of dissolved CO_2 molecules, P_{CO_2} is the partial pressure of CO_2 molecules in the vapor phase, and k_H is the Henry's law constant. For a given gas, k_H is strongly temperature-dependent. The lower the temperature, the higher the Henry's law constant, and, therefore, the higher the solubility. In Champagne and sparkling wines, Agabaliantz thoroughly examined the solubility of dissolved CO_2 molecules as a function of both temperature and wine parameters (*3*). His empirical relationships are still in use by today's Champagne makers. For a typical sparkling wine elaborated according to the "méthode champenoise", Agabaliantz established the temperature dependence of the Henry's law constant, which is displayed in **Table 1**. Once the champagne has undergone the second alcoholic fermentation, the pressure under the cork is ∼6 atm (at 12 °C). Following Henry's law with the data reported

† Telephone (33)3 26 91 86 14; fax (33)3 26 91 33 40; e-mail gerard.liger-belair@univ-reims.fr.

10.1021/jf048259e CCC: $30.25
Published on Web 03/18/2005

Table 1. Henry's Law Constant as a Function of Temperature for a Champagne with 12.5% (v/v) of Ethanol and 10 g/L of Sugars [Compiled from the Data of Agabaliantz (*3*)]

temp (°C)	Henry's law constant, k_H (kg/m^3/atm)	temp (°C)	Henry's law constant, k_H (kg/m^3/atm)
0	2.98	13	1.86
1	2.88	14	1.79
2	2.78	15	1.73
3	2.68	16	1.67
4	2.59	17	1.60
5	2.49	18	1.54
6	2.41	19	1.48
7	2.32	20	1.44
8	2.23	21	1.40
9	2.16	22	1.34
10	2.07	23	1.29
11	2.00	24	1.25
12	1.93	25	1.21

by Agabaliantz, it can be deduced that the champagne may contain ~11.8 g/L of dissolved CO_2.

Thermodynamically speaking, the behavior of Henry's law constant as a function of temperature can be conveniently expressed with a van't Hoff-like equation

$$k_H = k_{298K} \exp\left[-\frac{\Delta H_{diss}}{\mathcal{R}}\left(\frac{1}{\theta} - \frac{1}{298}\right)\right] \quad (3)$$

where ΔH_{diss} is the dissolution enthalpy of CO_2 molecules in Champagne (in J/mol), $\mathcal{R}$ is the ideal gas constant (8.31 J/K), and θ is the absolute temperature (in K). By fitting Agabaliantz data with the latter equation, it is worth noting that the dissolution enthalpy of CO_2 molecules in Champagne may be evaluated. The best fit to Agabaliantz data was found with $\Delta H_{diss} \approx 24800$ J/mol (see **Figure 1**). To the best of our knowledge, this is the first attempt to evaluate the dissolution enthalpy of CO_2 molecules in Champagne. In comparison, the dissolution enthalpy of CO_2 molecules in pure water is ~19900 J/mol (*4*).

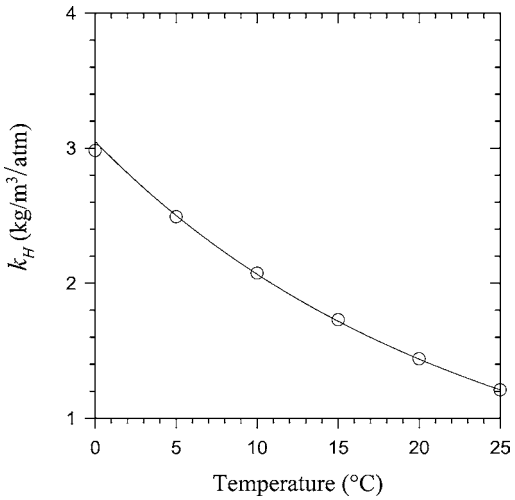

Figure 1. Henry's law constant as a function of temperature (○) [redrawn from Agabaliantz data (*3*)]. Dashed line is the best fit to the Agabaliantz data, drawn with the van't Hoff-like eq 3 and with $\Delta H_{diss} \approx 24800$ J/mol.

From the point of view of the chemist, Champagne can indeed be viewed as a multicomponent aqueous solution. The chemical composition of a typical Champagne wine is reported in **Table 2** (*5*). Actually, gases such as CO_2 undergo specific reactions

Table 2. Average Composition of a Typical Champagne Wine[a]

compound	quantity
ethanol	≈12.5% v/v
CO_2	10–12 g/L
glycerol	≈5 g/L
tartaric acid	≈2.5–4 g/L
lactic acid	≈4 g/L
sugars	10–50 g/L
proteins	5–10 mg/L
polysaccharides	≈200 mg/L
polyphenols	≈100 mg/L
amino acids	0.8–2 mg/L
volatile organic compounds (VOC)	≈700 mg/L
lipids	≈10 mg/L
K^+	200–450 mg/L
Ca^{2+}	60–120 mg/L
Mg^{2+}	50–90 mg/L
SO_4^{2-}	≈200 mg/L
Cl^-	≈10 mg/L

[a] Typically, pH ≈3.2 and the ionic strength is 0.02 M (*5*).

with water. Equilibrium is established between the dissolved CO_2 and H_2CO_3, the carbonic acid.

$$(CO_2)_{aq} + H_2O \leftrightarrow H_2CO_3 \quad (4)$$

Moreover, carbonic acid is a weak acid that dissociates in two steps (*6*).

$$H_2CO_3 + H_2O \leftrightarrow H_3O^+ + HCO_3^- \qquad pK_{a1}\,(\text{at } 25\ ^\circ\text{C}) = 6.37 \quad (5)$$

$$HCO_3^- + H_2O \leftrightarrow H_3O^+ + CO_3^{2-} \qquad pK_{a2}\,(\text{at } 25\ ^\circ\text{C}) = 10.25 \quad (6)$$

However, as the pH of Champagne is relatively low (~3.2), no carbonated species (CO_3^{2-}, HCO_3^-) should coexist with dissolved CO_2. Very recently, the ^{13}C magnetic resonance spectroscopy (MRS) technique was used as an unintrusive and nondestructive method to determine the amount of CO_2 dissolved in a closed bottle of Champagne or sparkling wine (*7*). Different well-separated peaks were recorded in a ^{13}C spectrum, as can be seen in **Figure 2**: (i) the quadruplet of the CH_3 group of ethanol appears at 17.9 ppm, (ii) the triplet of the $CH_2(-OH)$ group of ethanol appears at 57.3 ppm, and (iii) the singlet of CO_2 appears at 124.4 ppm, thus confirming the absence of other carbonated species (CO_3^{2-}, HCO_3^-) in the liquid matrix.

2.2. Uncorking the Bottle Breaks the Thermodynamic Equilibrium of CO_2. When the bottle is opened, the partial pressure of CO_2 in the headspace falls. Therefore, the CO_2 concentration in Champagne is no longer in equilibrium with its partial pressure in the vapor phase. The wine enters a metastable state; that is, it contains CO_2 molecules in excess in comparison with what Henry's law states. To recover a new stable thermodynamic state corresponding to the partial pressure of CO_2 molecules in the atmosphere (only ~0.0003 atm), almost all of the carbon dioxide molecules dissolved into the Champagne must escape. The Champagne becomes supersaturated with CO_2, as schematized in **Figure 3**. Before proceeding further, it is important to define the supersaturating ratio, used for quantifying CO_2 molecules in excess in a carbonated liquid. The supersaturating ratio S is defined as (*8*)

$$S = (c_L/c_0) - 1 \quad (7)$$

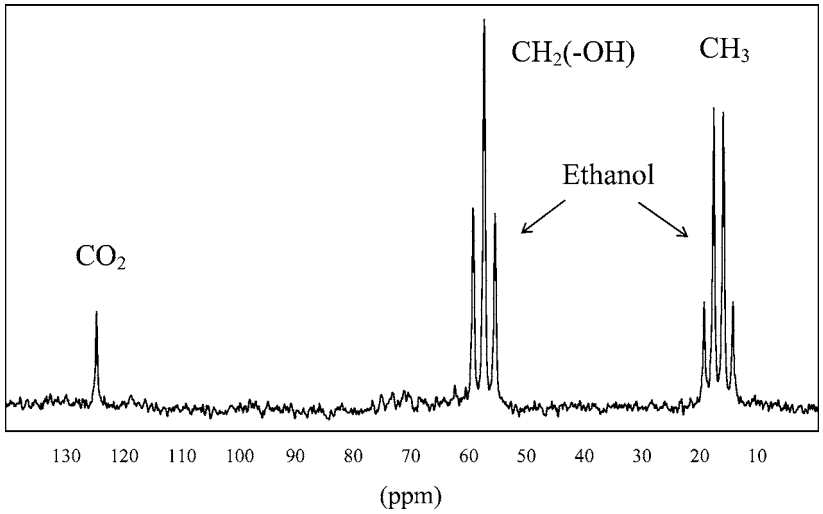

Figure 2. ^{13}C spectrum recorded to measure CO_2 concentration in Champagne (*7*). It is clear that no carbonated species (CO_3^{2-}, HCO_3^-) coexist with dissolved CO_2.

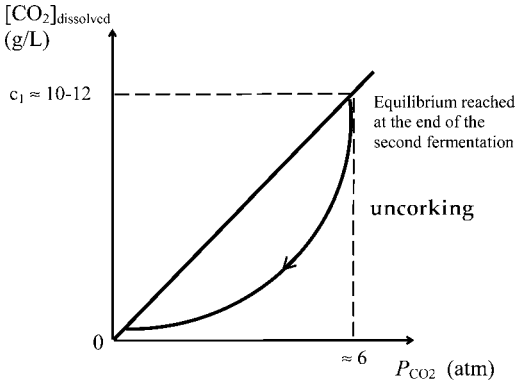

Figure 3. As stated by Henry's law, the concentration of CO_2 molecules dissolved into the Champagne is proportional with the partial pressure of CO_2 in the vapor phase under the cork. After the bottle is uncorked, the partial pressure of CO_2 falls and the thermodynamic equilibrium of the closed bottle is broken. Champagne becomes supersaturated with carbon dioxide molecules, which must escape from the liquid medium.

where c_L is the concentration of CO_2 in the liquid bulk and c_0 is the equilibrium concentration corresponding to a partial pressure of gaseous CO_2 of 1 atm.

As soon as $S > 0$, a liquid enters a metastable state and must degas to recover a supersaturating ratio equal to zero. In the case of Champagne wines, just after the bottle is uncorked, c_L is the equilibrium concentration of CO_2 in the liquid bulk corresponding to a partial pressure of CO_2 of ~6 atm. Because there is a strict proportionality between the concentration of dissolved gas and its partial pressure in the vapor phase (as expressed by Henry's law), $c_L/c_0 \approx 6$. Therefore, just after the bottle is uncorked, the supersaturating ratio of Champagne is ~5, and the Champagne must degas.

Actually, the escape of 10 g of CO_2 dissolved molecules per liter of Champagne is equivalent to a volume of gaseous carbon dioxide of ~6 L at 20 °C (as the molar volume of an ideal gas is ~25 L/mol). If we make the assumption that a classic Champagne flute contains ~0.1 L of Champagne, we can estimate that ~0.6 L of gaseous carbon dioxide must escape from it to regain equilibrium. To get an idea of how many bubbles it involves, let us divide that volume by that of an average bubble of ~500 μm in diameter. A huge number of bubbles close to 10 million is found.

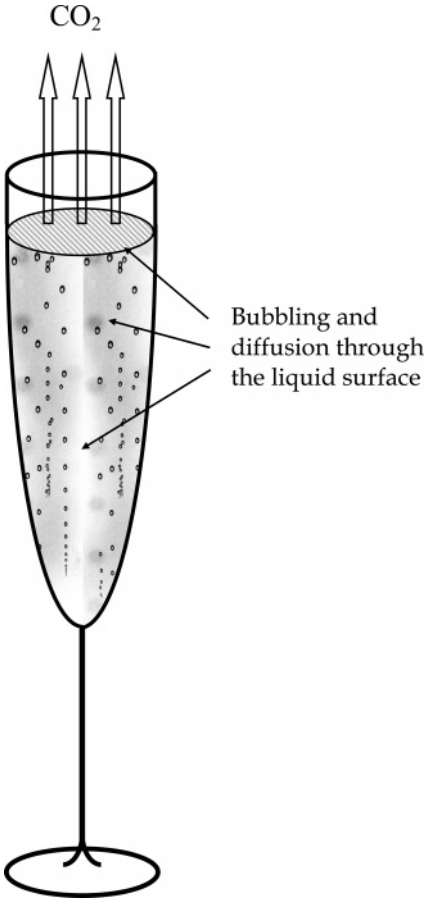

Figure 4. Two means of gas discharge, in a flute poured with Champagne.

Actually, there are two mechanisms for gas loss: losses due to diffusion through the surface of the liquid (invisible to the naked eye) and losses due to bubbling (effervescence) (see **Figure 4**). Recent experiments proved that in a classic crystal flute, contrary to what could have been expected, only ~20% of carbon dioxide molecules escape in the form of bubbles, whereas the other 80% escape directly through the free surface of the Champagne (*9*). Thus, if you were to leave your glass of Champagne alone, ~2 million carbon dioxide bubbles would escape from your flute. But, how and where do these bubbles form?

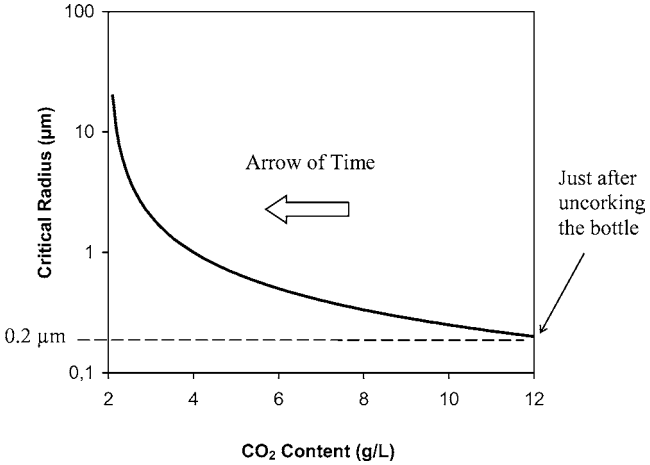

Figure 5. During the gas-discharging process, the critical radius below which bubble production becomes thermodynamically impossible progressively increases; thus, nucleation sites become in turn inactive, in increasing order of the bubble embryo trapped inside the particles acting as nucleation sites.

3. BUBBLE NUCLEATION

3.1. Critical Radius Required for Bubble Production. Actually, homogeneous nucleation within the liquid bulk and heterogeneous nucleation on molecularly smooth surfaces require very high supersaturating ratios that are totally unrealistic in the case of carbonated beverages. Wilt (*10*) obtained theoretically that supersaturating ratios over 1000 should be required for homogeneous nucleation at room temperature. In the case of liquids with low supersaturating ratios, such as sparkling wines and carbonated beverages in general, bubbles need pre-existing gas cavities larger than a critical size to overcome the energy barrier and grow freely (*11*, *12*). The critical radius r^* required to enable bubble production in a carbonated beverage is expressed as (see ref *9* and references cited therein)

$$r^* \approx 2\sigma/P_0S \qquad (8)$$

where σ is the surface tension of the liquid medium [of the order of 50 mN/m in Champagne and sparkling wines (*5*)]. At the opening of a Champagne bottle, because $S \approx 5$, the critical radius required is of the order of 0.2 μm. Jones et al. (*11*) suggested a new classification for the broad range of bubble formation often encountered. Production of bubbles from an existing gas cavity with a radius larger than the above-mentioned critical radius is referred as type IV nucleation.

Consequently, bubble formation in a glass of sparkling wine can take place only at a pre-existing gas cavity (with a radius of curvature larger than r^*) attached to a solid immersed in the bulk of the liquid or stuck on the glass wall. Equation 8 also tells us that the critical radius required to enable bubble formation from pre-existing gas cavities is not fixed. It actually changes over the passage of time within a glass of Champagne. Actually, it is inversely proportional to the supersaturating ratio S and, therefore, to the dissolved carbon dioxide content in the Champagne. Due to bubbling and diffusion through the surface of Champagne, CO_2 molecules progressively escape from the liquid. Subsequently, the dissolved carbon dioxide content c_L in the liquid medium progressively decreases, and as a result, the corresponding critical radius r^* required for bubble formation increases (see **Figure 5**). Consequently, bubble production stops in all of the particles acting as nucleation sites, with the largest sized sites ceasing production last.

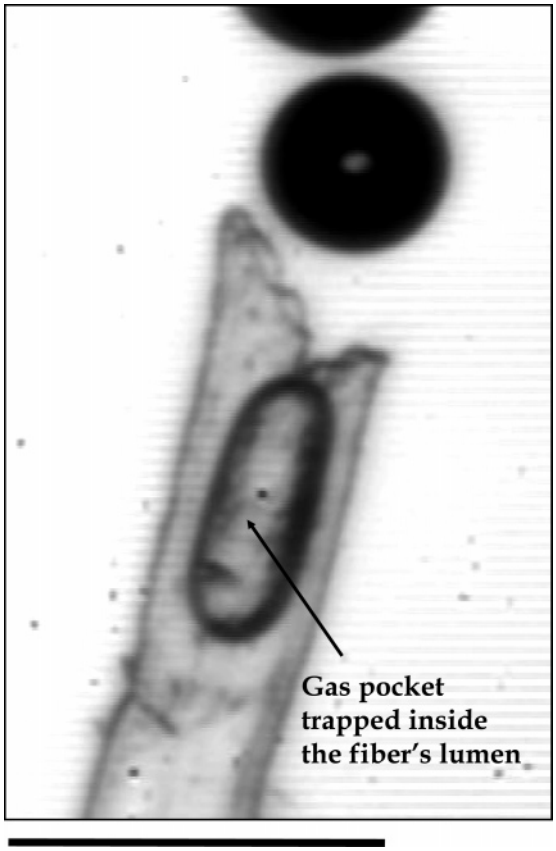

Figure 6. Close-up on a cellulose fiber acting as a bubble nucleation site (courtesy of Cédric Voisin). The fiber wall consists of closely packed cellulose microfibrils oriented mainly in the direction of the fiber. For a current review on the molecular and supramolecular structure of cellulose, see the paper by O'Sullivan (*20*) and references cited therein. Bar = 100 μm.

3.2. Close-up on Bubble Nucleation. Those gas-filled sites required for bubble production are generated when the liquid flows over the wall, during the filling of the flute. Contrary to general assumption, in Champagne, sparkling wines, beers, and carbonated beverages in general, nucleation sites are not located on irregularities of the glass itself, as was nevertheless assumed in some previous works (*13*−*15*). In liquids with low supersaturating ratios such as carbonated beverages, the length scale of glass irregularities is far below the critical radius of curvature required for the type IV nucleation process (*16*). Recently, the Champagne bubble production process in real consumption conditions, that is, in a glass, was directly and accurately filmed at a millisecond time scale at a quasi-micrometric resolution, with a high-speed video camera fitted with a microscope objective (*17*, *18*). It was clearly shown that most nucleation sites are located inside hollow and roughly cylindrical cellulose fibers that fell out of the air or remained from the dry-wiping process. Because of their geometry, these exogenous particles cannot be completely wetted by the liquid and are thus able to entrap gas pockets when the glass is filled. Gas pockets trapped inside the particles and plunged in the supersaturated Champagne start the repetitive bubble production process by diffusion of CO_2 molecules from the Champagne bulk to the gas pocket through the fiber wall (*19*). The hollow cavity where the gas pocket is trapped is denoted the "lumen" (see **Figure 6**).

3.3. Bubble Formation Frequencies. As a result of supersaturating, a difference of CO_2 concentration appears between the liquid bulk and the boundary layer in equilibrium with the CO_2 gas in the pre-existing gas pocket. Therefore, CO_2

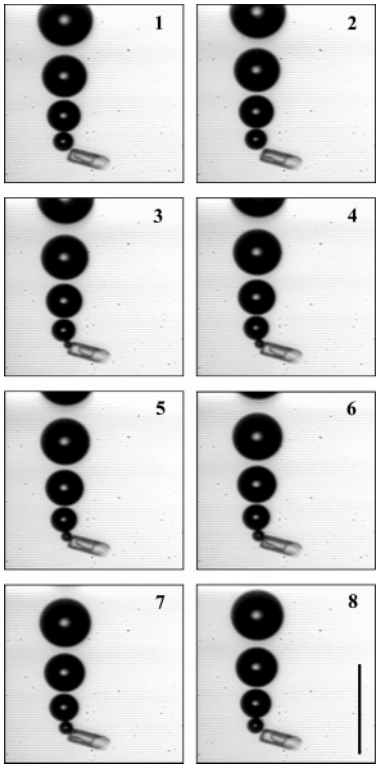

Figure 7. Typical time sequence illustrating one period of the repetitive bubble nucleation process. The time interval between two frames is ~10 ms. Bar = 100 μm.

molecules diffuse from the bulk to the gas pocket. A bubble forms and grows from this nucleation site. When buoyancy overcomes the vertical component of the capillary force anchoring the bubble to the cavity, it will detach, thereby providing an opportunity for a new bubble to form, grow, and detach at the same size, and so on, until bubble production stops through lack of dissolved gas. As a result, bubbles are released from nucleation sites with clockwork regularity. Bubbles rising in-line in a glass poured with Champagne are therefore the result of the cycle of bubble production, as shown in the time sequence displayed in **Figure 7**. The cyclic bubble production at a given nucleation site is characterized by its bubbling frequency, that is, the number of bubbles produced per second, a figure that can be illustrated using a stroboscope. When the strobe's flash frequency equals that of bubble production, the bubble train appears to be frozen to the naked eye (*15*).

It was noted that in the same flute and at the same time, a huge variation of the bubble formation frequency may be observed from one site to another. Actually, for a given nucleation site, the period needed for a bubble to grow from its embryonic size to its detachment size (~10−50 μm in diameter) depends on the inner geometrical properties of the microcavity. As a result, the frequency of bubble formation depends on the size and shape of the pre-existing microcavity. Therefore, assuming a collection of pre-existing microcavity shapes and sizes on the glass wall, one can observe in the same flute and at the same time various bubble trains with various bubble formation frequencies (*15*) (see, for example, the photograph displayed in **Figure 8**, which presents three bubble trains with three different bubbling frequencies, in the same flute and at the same time).

Concerning all of the observations of individual regular bubble trains conducted with strobe lighting, it was concluded that in a glass of Champagne, the distribution of bubble

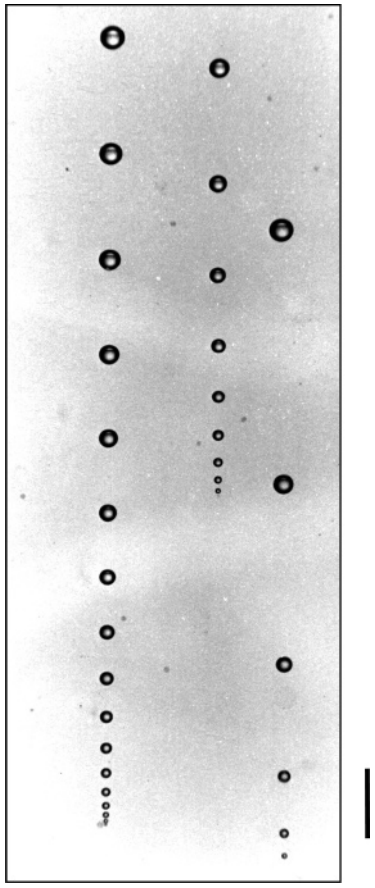

Figure 8. In the same flute and at the same time, because a collection of particle shapes and sizes exists on the glass wall, bubble trains with various bubble formation frequencies may be observed. Bar = 1 mm.

formation frequencies may be rather wide. Three minutes after pouring, frequencies ranging from <1 to 30 Hz were measured (*9*, *15*).

Because the kinetics of bubble formation depend also on the dissolved CO_2 content, bubble formation frequencies significantly vary from one carbonated beverage to another. In Champagne and sparkling wines, in which the gas content is ~3 times higher than that in beer, the most active nucleation sites were found to emit up to ~30 bubbles per second, whereas in beer, the most "active" nucleation sites produce up to only ~10 bubbles per second (*9*). Furthermore, because the content of dissolved CO_2 continuously decreases in a glass poured with Champagne (due to bubbling and diffusion through the free surface), the bubble formation frequency of a given nucleation site progressively decreases as time goes on until it finally stops due to a lack of dissolved gas (*9*, *17*).

4. BUBBLE RISE

4.1. Rising Velocities of Champagne Bubbles. A short examination of the three typical regular bubble trains presented in **Figure 8** is actually very instructive. The distance between two successive bubbles increases and, because bubbles are released from their respective nucleation site with clockwork regularity, it can be guessed that a bubble accelerates when rising through the liquid. The clockwork repetitive bubble production from nucleation sites was used to develop a simple setup, which consists of the association of a photo camera with a stroboscopic light, to follow the motion of bubbles in the flute poured with Champagne (*9*, *15*, *17*). Actually, because bubbles are released from nucleation sites with clockwork regularity, the photograph

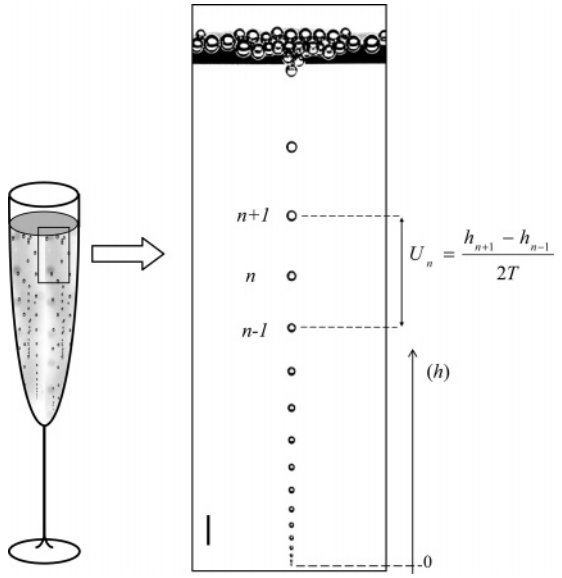

Figure 9. Determination of the rising velocity of bubbles during ascent from the enlarged photograph of a single bubble train and from the period of bubble production, *T*, as determined with strobe lighting (*15*). The velocity U_n of the *n*th bubble of the bubble train may be deduced from the position of the one that just precedes indexed *n*+1 and the one that just follows indexed *n*–1. Bar = 1 mm.

of each bubble train can be treated as a succession of pictures of the same bubble separated from the period of bubble formation, *T*, as determined by equaling the bubble formation frequency of a given bubble train with the frequency of strobe lighting. The velocity U_n of the *n*th bubble in the bubble train may then be simply deduced from the position of the one that just precedes, indexed $n+1$, and the one that just follows, indexed $n-1$, as schematized in **Figure 9**. The longest bubble trains were of the order of 10 cm. To eliminate the influence of the initial liquid convection when Champagne is poured into the glass, observation of the bubble trains (strobe lighting and photography) was conducted 3 min after pouring. Experiments were performed at room temperature (20 ± 2 °C).

In **Figure 10**, for rising bubbles of various bubble trains, the bubble velocity *U* was plotted as a function of its radius *R*. In **Figure 10**, *U*(*R*) is also superimposed with the well-known Stokes velocity, $U_{ST} = (2\rho g/9\eta)R^2$, where ρ and η are, respectively, the liquid density and viscosity and *g* is the acceleration due to gravity. The approximate Reynolds numbers experienced by ascending Champagne bubbles are also reported ($Re = 2\rho RU/\eta$). In terms of power law, **Figure 10** suggests a quadratic dependence with the radius for the velocity of rise. To a quite good approximation, it was found that the bubble velocity close to the glass wall can be modeled by a modification of the numerical prefactor in Stokes law:

$$U(R) = \frac{2\rho g\alpha}{9\eta}R^2 \quad (\text{with } \alpha \approx 0.6-0.8) \qquad (9)$$

More details about the determination of eq 9 can be found in Liger-Belair et al. (*21*).

4.2. Ascending Bubbles' Growth Rates. After release from the nucleation site, CO_2 molecules of the liquid continue to diffuse into the rising bubble. Hence, bubbles continue to increase in size when rising through the liquid as can be clearly seen in **Figure 10**. The bubble radius increase during the bubble rise was also determined from the setup described in the latter paragraph (*9*, *15*, *17*).

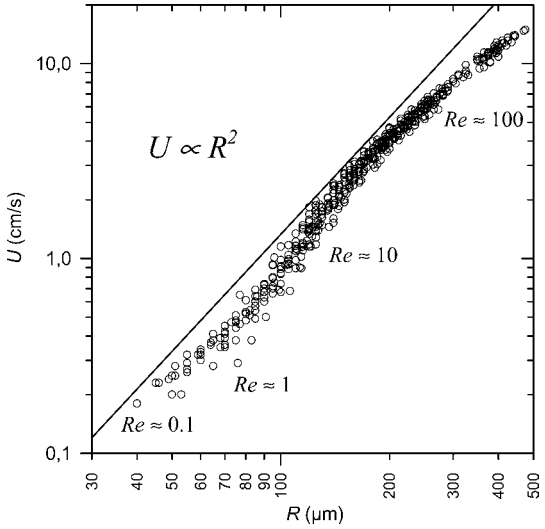

Figure 10. Velocity of ascending champagne bubbles plotted as a function of their radius, *U*(*R*): experimental data (○), compared with the well-known Stokes velocity (solid line), which constitutes a guide for the eyes. The approximate Re experienced by ascending bubbles is also reported close to the corresponding data.

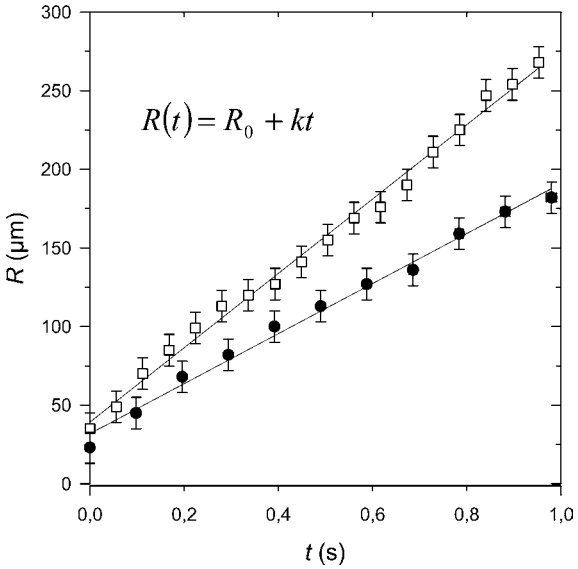

Figure 11. Bubble radius increase versus time for a bubble rising toward the liquid surface. Two typical bubble trains at different steps of gas discharge are considered.

Two typical time dependencies of bubble radii are presented in **Figure 11**. It appears clearly that, for each train, the bubble radius increases at a constant rate, $k = dR/dt$, when rising through the liquid. A constant bubble growth rate was also obtained for the other bubble trains considered. Thus

$$R(t) = R_0 + kt \qquad (10)$$

where R_0 is the bubble radius as it detaches from the nucleation site. R_0 is of the same order of magnitude as the radius of the mouth of the cellulose fiber, which acts as a nucleation site, that is, ∼10−20 μm (*17*, *18*). Three minutes after pouring, experiments conducted with Champagne and sparkling wines led to growth rates *k* ranging around ∼350−400 μm/s (*9*, *17*). Experiments were also performed with the growth rates of bubbles rising in beer glasses. In beer, 3 min after pouring,

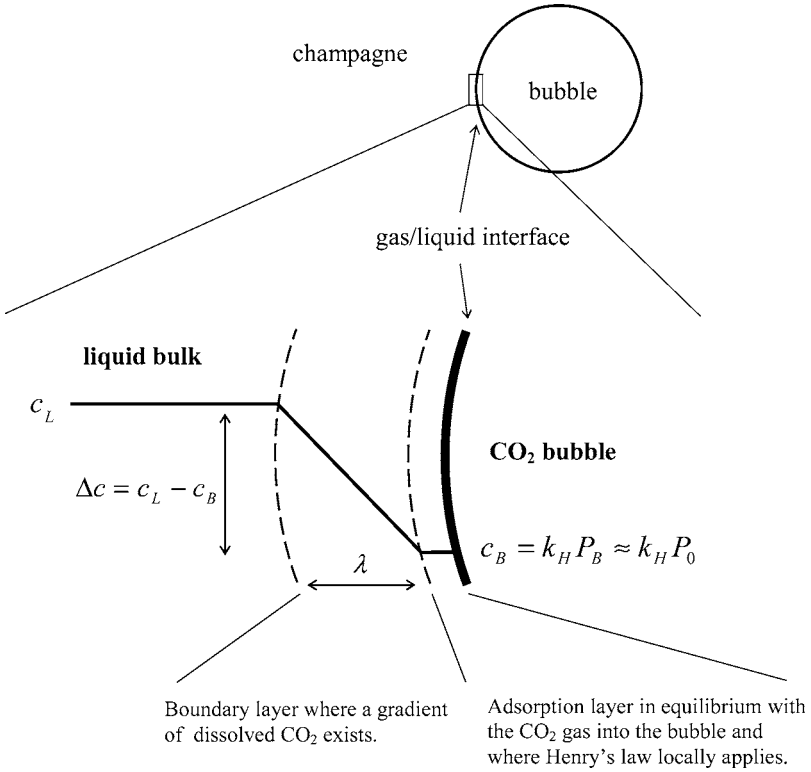

Figure 12. Carbon dioxide concentrations in the close vicinity of the CO_2 bubble surface.

bubble growth rates were found to lay ~100−150 μm/s, that is, ~3 times less than those in Champagne and sparkling wines (*9*).

With regard to the linearity of bubble radius increase with time, an explanation based upon mass transfer theory was proposed (*17*). The following theoretical bubble growth rate was obtained

$$k = \frac{dR}{dt} \approx 0.63 \frac{\mathcal{R}\theta}{P_B} D^{2/3} \left(\frac{2\alpha\rho g}{9\eta}\right)^{1/3} \Delta c \qquad (11)$$

where θ is the absolute temperature, $\mathcal{R}$ is the ideal gas constant, P_B is the pressure inside the rising bubble assumed to be equal to the atmospheric pressure P_0, D is the diffusion coefficient of CO_2 molecules through the liquid, ρ and η are, respectively, the liquid density and viscosity, g is the acceleration due to gravity, α is a numerical prefactor of ~0.7 for Champagne and sparkling wine bubbles, and ~0.5 for beer bubbles (*9*), and Δc (the driving force responsible for the diffusion of CO_2 into the rising bubble) is the difference in dissolved CO_2 concentrations between the liquid bulk and the close vicinity of the bubble surface in equilibrium with the gaseous CO_2 into the rising bubble (see **Figure 12**).

Strictly speaking, the pressure P_B inside the rising bubble is the sum of three terms: (i) the atmospheric pressure P_0, (ii) the hydrostatic pressure ρgh, and (iii) the Laplace pressure $2\sigma/R$ originated in the bubble's curvature. h is the depth at which the bubble rises, and σ is the surface tension of the liquid medium. However, as h varies from several millimeters to several centimeters, the surface tension of Champagne is of order of 50 mN m^{-1} (*5*), and bubbles' radii vary from several tens to several hundreds of micrometers, the contribution of both hydrostatic and Laplace pressures is clearly negligible with regard to the atmospheric pressure P_0. Therefore, $\Delta c = c_L - c_B \approx c_L - k_H P_0$. At 20 °C (see **Table 1**), $c_0 = k_{293K} P_0 \approx 1.44$g/L ≈ 32.7 mol/m^3. In Champagne, c_L being of the order of 10 g/L, it can be deduced that $\Delta c \approx 8.5$ g/L ≈ 193 mol/m^3.

Table 3. Some Physicochemical Parameters of Champagne and Beer

	Champagne	beer
viscosity[a] η ($\times 10^{-3}$ kg·m^{-1}·s^{-1})	1.48 ± 0.02	1.57 ± 0.02
surface tension[b] σ (mN/m)	46.8 ± 0.6	43.5 ± 0.5
density ρ (kg/m^3)	998	1003
CO_2 diffusion coefficient[c] D ($\times 10^{-9}$ m^2·s^{-1})	1.41	1.44

[a] Measured with an Ubbelhode capillary viscosimeter (*21*). [b] Measured with a pendant drop apparatus (Krüss) (*21*). [c] Measured by NMR (*22*).

As far as Champagne wines are concerned, the bubble growth rate k is very important, because this rate determines the bubbles' final average size—and this, in turn, is a hallmark of the wine's quality. It is thus important to better understand the role played by each parameter found in eq 11. Because Champagne bubbles were often compared with bubbles in beer, some classical physicochemical parameters of a standard commercial Champagne and beer were measured. They are displayed in **Table 3**.

Let us test the applicability of relationship 11 in the case of expanding Champagne bubbles at 20 °C. By using known values of ρ and η in Champagne, $\alpha = 0.7$, $D_{Champ} \approx 1.4 \times 10^{-9}$ m^2/s, and the difference in CO_2 concentrations between the liquid bulk and the close vicinity of the bubble surface, $\Delta c \approx 8.5$ g/L ≈ 193 mol/m^3, one finds

$$k \approx 0.63 \times \frac{8.31 \times 293}{10^5} \times (1.4 \times 10^{-9})^{2/3} \times \left[\frac{2 \times 0.7 \times 10^3 \times 9.8}{9 \times 1.5 \times 10^{-3}}\right]^{1/3} \times 193 \approx 370\ \mu\text{m/s}$$

which is in quite good accordance with the order of magnitude of observed growth rates (*9*, *14*).

At $\theta = 20$ °C, in Champagne and beer, the diffusion coefficient of CO_2 molecules D turned out to be very close. Moreover, at $\theta = 20$ °C, the dynamic viscosities of Champagne and beer were measured and found to be significantly different,

although quite close and $\sim 1.5 \times 10^{-3}$ kg/m/s. Finally, eq 11 shows that the diffusion coefficient D of CO_2 molecules, as well as the liquid viscosity and density η and ρ cannot account for different bubble growth rates k as observed between Champagne and beer and as can also even be observed between some Champagne and sparkling wines. Therefore, differences with Δc (i.e, the carbon dioxide content) were strongly suspected as being the main cause for observing different bubble growth rates among various beverages. According to eq 11, bubble growth rates should be directly proportional to the carbon dioxide content, through the parameter Δc. Actually, it is well-known that classical beer contains ~ 3 times less dissolved CO_2 than Champagne and most sparkling wines elaborated according to the méthode champenoise. Now, 3 min after pouring, experiments conducted with ascending beer bubbles led to growth rates $k \sim 3$ times less than those in Champagne and sparkling wines [$\sim 100-150$ μm/s in beer versus $\sim 350-400$ μm/s in Champagne and sparkling wines (*9*)], thus confirming the likely proportionality between k and Δc.

4.3. Relative Influence of Some Parameters on Average Bubble Size. The consumer pays much attention to the size of bubbles as they reach the liquid surface. This final average bubble size depends on several parameters, such as (i) the growth rate k during ascent, (ii) the bubble velocity U, and (iii) the distance traveled h by the bubble from its nucleation site. Now, because the time of ascent of a Champagne bubble is very short (≈ 1 s), the bubble growth rate k during ascent is constant during the bubble rise. Therefore, the rate of increase of the bubble radius with h becomes

$$k = \frac{dR}{dt} = \frac{dR}{dh}\frac{dh}{dt} = \frac{dR}{dh}U, \quad \text{i.e.,} \frac{dR}{dh} = \frac{k}{U} \tag{12}$$

Combining eqs 12 and 9 and performing the integration lead to

$$R = \left({R_0}^3 + \frac{27\eta k}{2\rho g \alpha}h\right)^{1/3} \tag{13}$$

By neglecting R_0, which is only of order of $10-20$ μm, the latter expression transforms as

$$R \approx 3\left(\frac{\eta}{2\alpha\rho g}kh\right)^{1/3} \tag{14}$$

In **Figure 13**, for bubbles of various bubble trains, and all along the bubble rise, experimental bubbles' radii were plotted versus the product kh. Experimental data were also compared with the latter theoretical expression (eq 14), where ρ, η, α, and g were replaced by their known values (see **Table 3**). The very good agreement between eq 14 and our experimental data corroborates both the bubble ascent and the bubble growth during the rise developed in sections 4.1. and 4.2.

By replacing in eq 14, the theoretical relationship 9 for the bubble growth rate k developed in section 4.2, the following dependence of the bubble radius with some of the liquid parameters was derived:

$$R \approx 1.24\left(\frac{9\eta}{2\alpha\rho g}\right)^{2/9}\left(\frac{\mathscr{R}\theta}{P_B}\right)^{1/3} D^{2/9}(c_L - c_B)^{1/3}h^{1/3} \tag{15}$$

To go further with the dependence of bubbles' radii with some parameters, we can also replace in eq 15 the diffusion coefficient D by its theoretical expression approached through the well-known theoretical Stokes−Einstein equation ($D \approx k_B\theta/6\pi\eta r$) (*23*), where k_B is the Boltzman constant (1.38×10^{-23} J/K) and r is the order of magnitude of the molecule's hydrodynamic radius (of the order of 10^{-10} m for the CO_2 molecule). The following relationship expressed in the MKSA system was thus obtained:

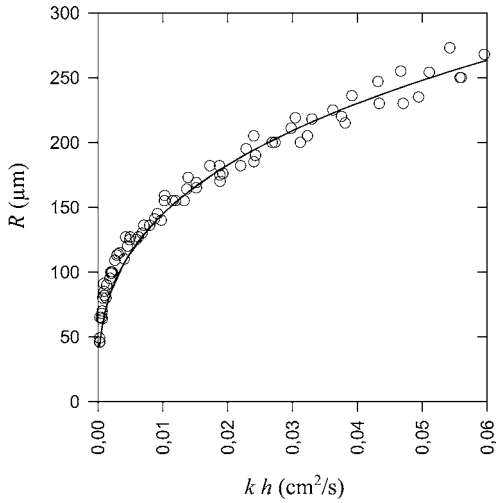

Figure 13. For various bubbles of various bubble trains, the radius of ascending bubbles is plotted versus the product of the growth rate k (expressed in cm/s) by the traveled distance h (expressed in cm). Experimental data (○) are compared with the theoretical relation expressed by eq 14 (solid line).

$$R(h,\theta,...) \approx 2.5\left(\frac{3k_B}{4\pi\alpha r}\right)^{2/9}\left(\frac{1}{\rho g}\right)^{2/9}\left(\frac{1}{P_B}\right)^{1/3}\theta^{5/9}(c_L - c_B)^{1/3}h^{1/3} \tag{16}$$

It is worth noting that the dependence of the bubble size with the liquid viscosity vanishes. Finally, by replacing in eq 16, k_B, α, and r by their known numerical values and by developing c_B as $k_H P_B$, one obtains

$$R(h,\theta,...) \approx 2.7 \times 10^{-3}\theta^{5/9}\left(\frac{1}{\rho g}\right)^{2/9}\left(\frac{c_L - k_H P_B}{P_B}\right)^{1/3}h^{1/3} \tag{17}$$

Furthermore, because the liquid density ρ does not significantly vary from one Champagne to another (and even from one carbonated beverage to another), we will discuss and emphasize the following several parameters: (i) the traveled distance h, (ii) the liquid temperature θ, (iii) the gravity acceleration g, (iv) the pressure inside the rising bubble P_B, and (v) the carbon dioxide content c_L.

(i) The longer the traveled distance h, the larger the bubble size, but the exponent being quite slow (1/3) means that the growing of the bubble mainly concerns the early stages of its ascent. By doubling the traveled distance, the bubble radius enhances by only 25%. We could therefore significantly increase the flutes' height without drastically modifying the bubbles' size.

(ii) In eq 17, the temperature appears directly as $\theta^{5/9}$, but we should not forget that the Henry's law constant k_H is also strongly temperature-dependent (see **Figure 1**) and conveniently expressed by the van't Hoff equation (eq 6). The temperature being expressed in Kelvin, the temperature dependence of the bubble size is nevertheless quite weak. Increasing the liquid temperature by 10 K (let us say from 278 to 288 K, which is approximately the range of Champagne tasting temperature) makes bubbles grow only $\sim 5-6\%$ in diameter.

(iii) The gravity acceleration, which is the driving force behind the bubble rise (through buoyancy), plays also a quite important role in the final bubble's size. This could indeed be easily evidenced during a parabolic flight where the acceleration

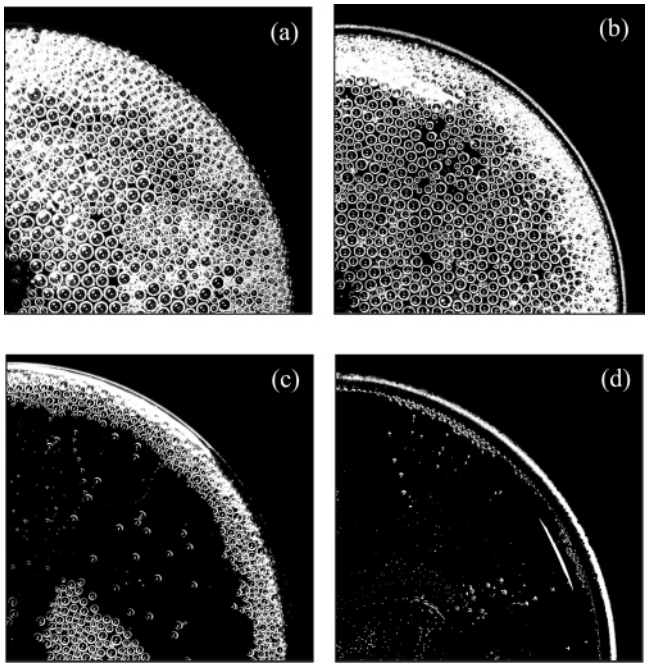

Figure 14. Time sequence showing top views of a flute poured with Champagne and followed as time proceeds: (**a**) immediately after pouring, (**b**) 3 min after pouring, (**c**) 10 min after pouring, and (**d**) 25 min after pouring. It clearly appears that the average bubbles' size decreases as time proceeds, as does the average number of floating bubbles.

changes from microgravity (close to 0*g*) to macrogravity (up to 1.8*g*). On the moon, for example, where the gravity is about one-sixth that of the Earth's, the average bubbles' size would increase by ~50% in diameter (and therefore by a factor of >3 in volume).

(iv) The pressure inside the rising bubble is equivalent to the atmospheric pressure P_0 (for the reasons detailed in the latter paragraph). Usually, at sea level, this pressure is equivalent to 1 atm (or 10^5 N/m^2). Reducing the atmospheric pressure to only 0.3 atm (on the top of Mount Everest, for example) would increase the average bubble diameter by ~55% (and therefore by a factor of almost 4 in volume). This is basically the same phenomenon that is responsible for gas embolism in divers who have breathed high-pressure air under water if they resurface too quickly.

(v) The carbon dioxide content of the liquid medium c_L also influences the final average bubbles' size. Reducing c_L by a factor of 3 (which is approximately the factor between Champagne and beer) would decrease the average bubble size by ~40% (i.e., by ~80% in volume). Moreover, after a given Champagne is poured into a flute, due to bubbling and diffusion through the surface of the Champagne, CO_2 molecules progressively escape from the liquid. Subsequently, the dissolved carbon dioxide content c_L in the liquid medium progressively decreases. Therefore, as time proceeds during Champagne tasting, the average bubbles' size at the liquid surface progressively decreases, as can be seen in the sequence displayed in **Figure 14**.

4.4. Influence of Surface-Active Macromolecules of Champagne on Drag Coefficient of Ascending Bubbles. As first noted by Bond (*24*), the hydrodynamics of rising bubbles strongly depends on the presence of surface-active substances in the liquid medium. During ascent, surface-active materials progressively accumulate at the rear part of a rising bubble, thus increasing the immobile area of the bubble surface. It ensures a gradient of surface tension $\nabla\sigma$ between the front and rear parts

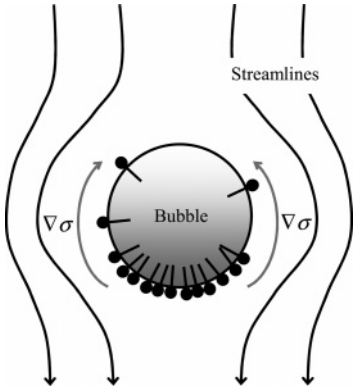

Figure 15. Liquid streamlines sweep surfactant molecules toward the bottom of a rising bubble, thus creating a gradient of surface tension $\nabla\sigma$ around the bubble interface. In turn, countercurrents raise along the bubble interface and lower its velocity of rise. This model based on the rigidification of the rear part of the bubble is known as the "stagnant-cap" model.

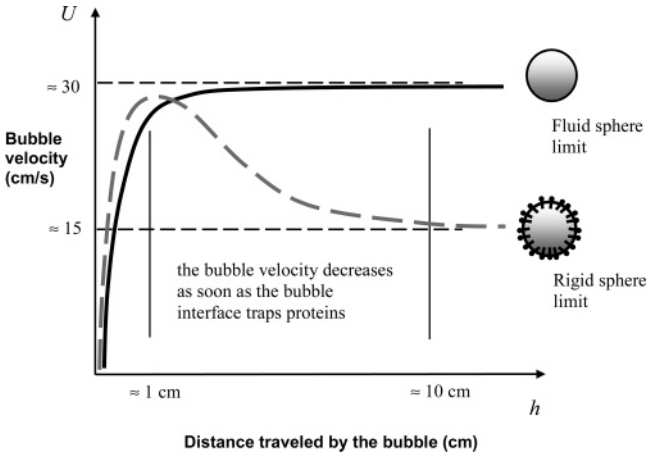

Figure 16. Velocity versus traveled distance of a millimetric bubble released in ultrapure water (black dashed line) and in water added with only 10 mg/L of BSA (gray dotted line) [redrawn from Ybert and di Meglio (*33*)].

of the bubble, which induces a modification of the hydrodynamic boundary conditions on the bubble via the onset of the so-called Marangoni effect (see **Figure 15**). The gradient of surface tension around the rising bubble induces a viscous shear stress, which reduces its interfacial mobility. Viscous dissipation is therefore enhanced, which leads to a lower rising velocity. This model based on the rigidification of the rear part of the bubble is known as the stagnant cap model. Numerous experimental, numerical, and theoretical researches on bubble motion have already confirmed this phenomenon (*24*−*34*). **Figure 16** illustrates this Marangoni effect, which progressively lowers the velocity of a millimetric bubble rising in water diluted with proteins. Hydrodynamically speaking, a rising bubble is rigidified by surfactants and runs into more resistance than a rising bubble presenting a more flexible interface free from surface-active materials. Therefore, the drag coefficient C_D experienced by a bubble of a fixed radius rising in a surfactant solution progressively increases because the surface of the stagnant cap progressively increases. Bubbles of fixed radii ascending in surfactant solutions therefore experience a transient regime, where the bubble behavior progressively changes from that of a fluid to that of a rigid sphere (as the bubble surface is completely rigidified by surfactants). Actually, there are surface-active substances in Champagne and sparkling wines likely to be adsorbed at the bubble surface, such as proteins and

Table 4. Relationships, Derived for both Rigid and Fluid Sphere Conditions, between the Drag Coefficient and the Reynolds Number of Ascending Bubbles

authors	range of validity	relationship for $C_D(Re)$[a]	bubble surface state
Schiller and Naumann [see Clift et al. (*39*)]	Re < 800	$C_{RS} = 24/Re(1 + 0.15Re^{0.687})$	rigid
Magnaudet et al. (*40*)	Re < 50	$C_{FS} = 16/Re(1 + 0.15\sqrt{Re})$	fluid
Maxworthy et al. (*41*)	1 < Re < 800	$C_{FS} = 11.1Re^{-0.74}$	fluid

[a] Subscripts RS and FS refer to rigid and fluid sphere boundary conditions, respectively.

glycoproteins (*35*−*38*). Such materials will certainly modify the bubble surface state during ascent and, therefore, the drag exerted on bubbles in comparison with the drag exerted on bubbles rising in a liquid free from surface-active compounds.

Finally, the drag coefficient of a single bubble rising in a liquid medium may be used to reveal whether the bubble interface is contaminated with surface-active substances.

4.5. Bubble Drag Coefficient during Ascent: Indirect Determination of Its Surface State. It is quite simple to measure the experimental drag coefficient C_D experienced by a rising bubble. The simultaneous measurements of the bubble velocity and of its radius allow a simple experimental determination of the drag coefficient experienced by a rising bubble through the expression

$$C_D = \frac{8gR}{3U^2} \tag{18}$$

Details about the determination of eq 18 can be found in ref *21*. During the past decades, many empirical or semiempirical equations have been proposed to approximate C_D for bubbles in free rise. Some of the most popular are listed in the book by Clift et al. (*39*). Our experimental measurements of $C_D(Re)$ are to be compared with the drag coefficients experienced by a bubble in the two limiting boundary regimes in terms of interfacial mobility (on the one hand, a rising bubble free from surface-active substances presenting a full interfacial mobility and, on the other hand, a contaminated bubble with a zero velocity boundary condition for the external fluid that hydrodynamically behaves as a rigid sphere of the same density and the same diameter). We therefore retrieved three empirical drag coefficients $C_D(Re)$, which are listed in **Table 4**.

To indirectly access the bubble surface state during the rise, the normalized drag coefficient C_D^* defined as follows was used:

$$C_D^* = \frac{(C_D - C_{FS})}{(C_{RS} - C_{FS})} \tag{19}$$

C_{RS} and C_{FS} are well-known empirical drag coefficients derived, respectively, for rigid and fluid sphere conditions (see **Table 4**). Therefore, bubbles with a fully mobile interface behaving hydrodynamically as fluid spheres will exhibit values of C_D^* close to 0, whereas polluted bubbles behaving hydrodynamically as rigid spheres will have values of C_D^* close to 1. In **Figure 17**, for bubbles of various bubble trains, the normalized drag coefficient was plotted as a function of the distance traveled for a bubble from its nucleation site, denoted *h*.

At low *h* ($h < 2-3$ mm), just after the bubble detachment from a nucleation site stuck on the glass wall, C_D^* is significantly higher than the rigid sphere limit. Actually, during the very first moments after detachment from the nucleation site, wall effects are certainly not negligible and probably modify the liquid flow around the rising bubble, resulting in a significant increase of the drag coefficient experienced by the bubble. Then,

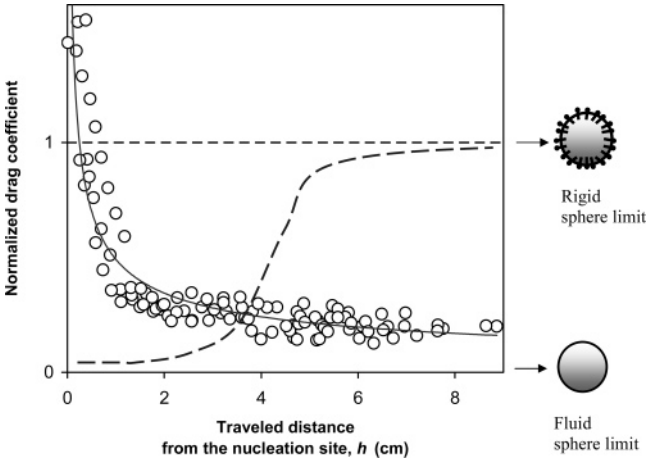

Figure 17. Normalized drag coefficient experienced by Champagne bubbles as a function of the distance they traveled from their nucleation site: experimental data (○); exponentially fitted curve (dashed line); behavior that a bubble of a fixed size would experience (long dashed line).

from $h \approx 3$ mm to $h \approx 1$ cm, C_D^* quickly decreases from the rigid sphere limit to an intermediate value close to the fluid sphere limit, thus suggesting that the Champagne bubble interface progressively increases its mobility. From $h \approx 1$ cm to $h \approx 10$ cm, C_D^* remains quite low, which suggests that Champagne bubbles have reached a quasi-stationary stage in terms of interfacial mobility. Strictly speaking, the level of the plateau seems to slightly decrease during this second quasi-stationary stage, which means that the bubble interface could continue to very progressively increase its mobility. In **Figure 17**, the line that progressively raises from the fluid to the rigid sphere limit qualitatively symbolizes the transient regime that a bubble of a fixed radius rising in a surfactant solution would experience.

In the present situation, the main features of experimental $C_D^*(h)$ in **Figure 17** strongly suggest that, contrary to a bubble with a fixed radius, the expanding Champagne bubble interface experiences a transient regime during its way up, where the bubble interface progressively changes its mobility from that of a rigid sphere to that of a fluid sphere. We are logically tempted to attribute this gain of interfacial mobility during ascent to the bubble growth, which continuously offers newly created surface to the adsorbed surface-active materials, thus diluting surface-active compounds on ascending bubbles.

4.6. Champagne Bubble Surface State Is Ruled by a Competition between Surfactant Adsorption and Bubble Growth. During ascent, surface-active substances accumulate at the bubble interface and contribute to its rigidifying, by increasing the amount of adsorbed materials. However, at the same time, the bubble continuously grows as a result of supersaturating. Therefore, the area of the bubble interface increases, thus diluting the amount of the adsorbed materials. Bubbles experience a competition between two opposing effects.

The parameter that controls the bubble surface state is its surface concentration of contaminants, denoted $\Gamma = M/A$, which is the ratio of the mass M of contaminants adsorbed to the bubble area A. The variation of the bubble surface concentration with time, on expanding bubbles, is governed by the following equation (*42*):

$$\frac{d\Gamma}{dt} = \underbrace{\frac{1}{A}\left(\frac{dM}{dt}\right)_A}_{\substack{\text{rate at which}\\ \text{surfactants adsorb}\\ \text{on the rising bubble}}} - \underbrace{\frac{M}{A^2}\left(\frac{dA}{dt}\right)_M}_{\substack{\text{rate of}\\ \text{dilatation of}\\ \text{the bubble area}}} \qquad (20)$$

Therefore, the variation with time of the surface concentration of contaminants on ascending bubbles depends on the ratio of the two terms in the right-hand side of eq 20. If the rate of dilatation of the bubble area exceeds the rate at which surface-active materials is transported to the bubble interface, the surface concentration of surfactants decreases and the bubble progressively cleans its surface. On the contrary, if the surfactant transport exceeds the dilution effect due to the bubble growth, the bubble interface is progressively "invaded" by surfactants and becomes rigid.

After the first nonstationary regime where $C_D^* > 1$, it appears clearly from **Figure 17** that the expanding Champagne bubbles experience a transient regime during ascent, where the bubble behavior progressively changes from that of a rigid sphere to that of a fluid sphere. As a result, it seems that the bubble growth quickly overcomes the adsorption rate of surface-active compounds on the ascending bubble. In a way, by continuously growing during ascent, Champagne bubbles would "clean up" themselves (*42*).

4.7. Could the Drag Coefficient Experienced by Bubbles Be Used as a Fingerprint of the Liquid They Are Rising in? Actually, the interplay of bubbles' growth, surface tension, and liquid viscosity, combined with the pool of surface-active macromolecules characteristic of a given carbonated beverage, could indeed be unique and therefore induce variations of bubbles' drag coefficients all along their rise peculiar to the liquid matrix they are rising through. Thus progressively emerged the idea that the thorough examination of bubbles' drag coefficients could be used as a sort of fingerprint of the liquid medium they are rising in.

Four different beverages were tested: one Champagne, two different sparkling wines (one Cava from Spain and one from Argentina), and a classical French beer. In **Figure 18**, in each of the four above-mentioned beverage, the normalized drag coefficient C_D^* experienced by expanding bubbles during ascent was plotted along their rise as a function of their increasing Reynolds number. From Re $\approx$ 10, it was found that beer bubbles behaved rather close to the rigid sphere limit during their rise toward the liquid surface. This observation suggests a complete coverage of the beer bubble interface with surfactants, thus confirming a result first described by Shafer and Zare (*43*). There are three main differences between Champagne and beer that may affect the rise of bubbles (*9*, *21*): (i) Beer, in general, contains much more protein (several hundreds of milligrams per liter) than Champagne does (only a few milligrams per liter); (ii) the dissolved gas content is $\sim$3 times lower in beer than in Champagne, and (iii) the ethanol content is higher in Champagne (12.5% v/v) than in beer ($\sim$5% v/v). Because beer contains $\sim$30 times more surface-active materials likely to be adsorbed at the bubble interface than Champagne, the much higher drag coefficient experienced by beer bubbles is certainly mainly due to an increase of the amount of surfactants collected during ascent. Furthermore, because the gas content is lower in beer, growth rates of beer bubbles are lower than those of Champagne (*9*). As a result, the dilution effect due to the rate of dilatation of the bubble area may be too weak to avoid the rigidification of the bubble interface in beer. Moreover, previous studies demonstrated that properties of adsorption layers on interfaces are very dependent on the ethanol content (*44*−*48*). As a result, the ethanol also probably affects the bubble rise. Experiments are to be conducted along that line to understand the role played by ethanol in the adsorption process during the bubble rise.

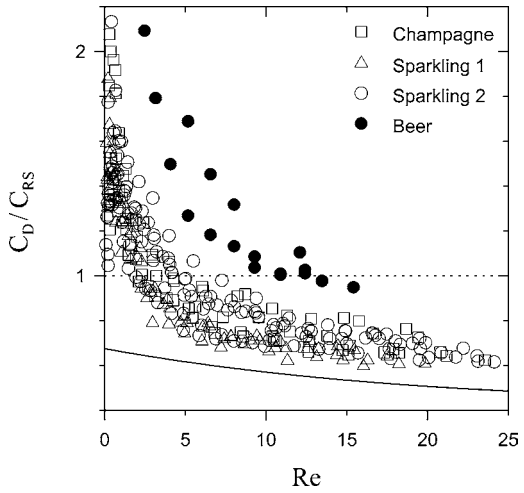

Figure 18. In each of the four tested beverages (a Champagne, two sparkling wines, and a beer), plot of the normalized drag coefficient C_D^* experienced by bubbles expanding along their rise as a function of their increasing Reynolds number: rigid sphere limit (dotted line); fluid sphere limit (dashed line).

Nevertheless, it seems to be quite difficult to detect significant differences between the Champagne and the two other sparkling wines. This first campaign of experiments on the drag experienced by bubbles was conducted with macrophotographs of bubble trains of several centimeters (like the one displayed in **Figure 9**, where the resolution of enlarged pictures was about $\pm$20 μm). Experiments are planned to investigate the drag coefficients experienced by bubbles in the very early stage of their rise (the first millimeter, where the Reynolds number is still lower than unity) and with a high-speed camera filming at 1000 frames/s with a quasi-micrometric resolution. With such a resolution, differences between various Champagnes and sparkling wines could eventually finally be underscored.

5. BUBBLE BURSTS

5.1. Bubble's Shape at the Liquid Surface. A Champagne bubble reaches the liquid surface with a size that depends on the distance traveled from its nucleation site (see section 4.3). Experimentally, it was observed that bubble diameters rarely exceed $\sim$1 mm. At the free surface, the shape of a bubble results from a balance between two opposing effects: the buoyancy F_B, of the order of $\rho g \pi R^3$, which tends to make it emerge from the liquid surface, and a capillary force F_c inside the hemispherical thin liquid film, of the order of $\sigma \pi R$, which tends to maintain the bubble below the liquid surface. In the case of Champagne millimetric bubbles, buoyancy will be neglected for capillary effects. Consequently, like a tiny iceberg, a bubble only slightly emerges from the liquid surface, with most of its volume remaining below the free surface (see **Figure 19**). The emerged part of the bubble, the bubble cap, is essentially a spherically shaped film of liquid, which gets thinner and thinner

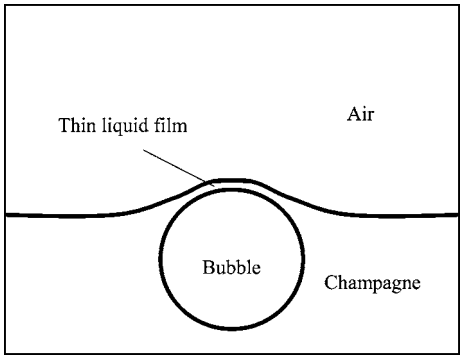

Figure 19. Like an iceberg, a Champagne bubble only slightly emerges from the liquid surface.

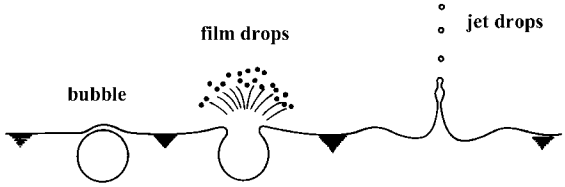

Figure 20. Scheme of the two production methods of droplets from a bursting bubble [redrawn from the paper by Resch et al. (*50*)].

as the liquid drains back into the liquid bulk. A bubble cap that has reached a critical thickness of ~100 nm (*49*) becomes so thin and sensitive to such disturbances as vibrations and temperature changes that it finally ruptures. For bubbles of millimeter size, the disintegration of the bubble cap takes from 10 to 100 μs. Then, a complex hydrodynamic process ensues, causing the collapse of the submerged part of the bubble and projecting into the air tiny droplets of liquid. This process is indeed characteristic of carbonated beverages in general.

5.2. Single Bubble Bursts. It is now generally recognized that bubbles bursting at a liquid surface eject two kinds of droplets (*50*): (i) small droplets called film drops, formed as the film of the emerged bubble cap disintegrates, and (ii) droplets formed by the collapse of the bottom of the bubble, called jet drops (see **Figure 20**). Nevertheless, it was shown that bubbles with a diameter of $<\sim$2 mm produce no film drops as they burst (*50*). Because the Champagne bubbles' diameter rarely exceeds ~1 mm as they reach the liquid surface, it can be concluded that only jet drops constitute the cloud of droplets above the liquid surface.

A reconstructed time sequence illustrating four stages of the collapse of a single Champagne bubble is presented in **Figure 21** (*51*). A brief description of each frame follows: In frame 1, a single bubble floats at the liquid surface. In frame 2, the bubble cap has just ruptured (on a time scale of 10−100 μs). During this extremely brief initial phase, the bulk shape of the bubble has been "frozen", and a nearly millimetric open cavity remains as a tiny indentation in the liquid surface. In frame 3, while collapsing, the bubble cavity gives rise to a high-speed liquid jet above the free surface. In frame 4, the upward liquid jet becomes unstable and finally breaks into jet drops. The number, size, and velocity of jet drops produced during bubble collapse depend on the size of the initial bursting bubble (*52*−*55*).

5.3. Possible Impact on the Flavor Perception in Sparkling Wines. Previous studies in other nonfood systems demonstrated that droplets issued from bursting bubbles commonly contain much higher concentrations of surface-active materials than those found in the liquid bulk, and especially in the field of oceanography where bursting bubbles play a crucial role in the global air/sea exchanges (*56*−*60*). Now, due to their amphiphilic

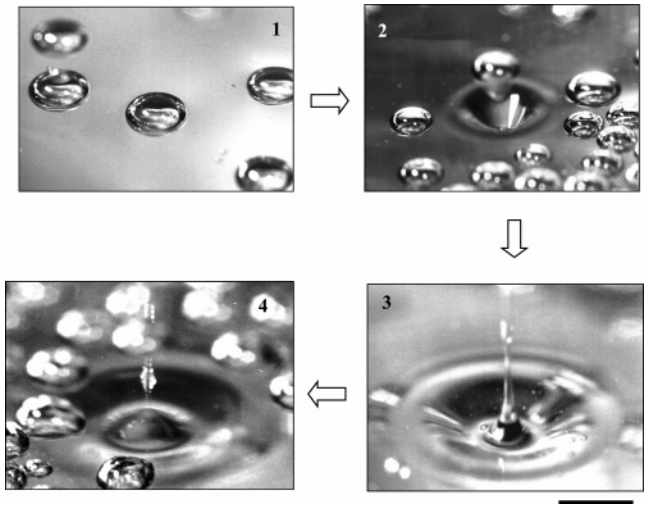

Figure 21. Reconstructed time sequence illustrating four stages of the collapse of a single bubble at the surface of a glass poured with Champagne. The time interval between frames 1 and 2 is about a few tens of microsecond, whereas it is about 1 ms between frames 2 and 3 and between frames 3 and 4. Bar = 1 mm.

structure, some of the various molecules of Champagne show surface activity, including, for example, alcohols (ethanol, butanol, pentanol, phenyl-2-ethanol, etc.), some aldehydes (butanal, hexanal, and hexenals), organic acids (propionic, butyric acid, etc.), and certain thiols. Actually, it was recently demonstrated that Champagne wines contain certain flavor-active volatile thiols (2-furanmethanethiol, benzenemethanethiol, and ethyl 3-mercaptopropionate) at concentrations considerably higher than their perception thresholds (*61*). These volatile thiols are expected to contribute to the empyreumatic nuance in the bouquet of old Champagne wines (*61*). Such more or less amphiphilic molecules are thus likely to be dragged along the bubble path, from its nucleation site to the free surface (*9*, *21*, *42*). Then, whatever is concentrated near the free surface of Champagne is likely to be ejected into the air on the droplets, thus contributing to the global sensorial perception of a sparkling wine.

5.4. Bubble Bursts in a "Bubble Raft". For a few seconds after pouring, the free surface of the liquid is completely covered with a bubble raft in constant renewal, where bubbles burst close to each other. Despite the large body of research concerned with collapsing bubble dynamics, the close-up observation of bubbles collapsing at the free surface of a glass poured with champagne nevertheless recently revealed an unexplored and visually appealing phenomenon. Actually, in an attempt to freeze the famous jets arising when Champagne bubbles collapse at the liquid surface by using classical high-speed macrophotography techniques, snapshots of bubbles collapsing close to each other were taken by accident (*62*, *63*).

Due to the extreme briefness of a bursting event, very few photographs froze snapshots of the collapsing process in a Champagne bubble raft in constant renewal. The photograph displayed in **Figure 22**, for example, was taken a few seconds after Champagne was poured into the flute. Clearly, bubbles adjacent to the bubble-free central area are literally sucked toward the now empty cavity left by a central bubble that has just ruptured, thus suggesting violent stresses in the thin films of neighboring deformed bubble caps. Because we are dealing with bubbles collapsing at a free liquid/gas interface, we are logically tempted to wonder about the dynamics of the famous jet arising after the bubble collapse. Does it exist, as in the single

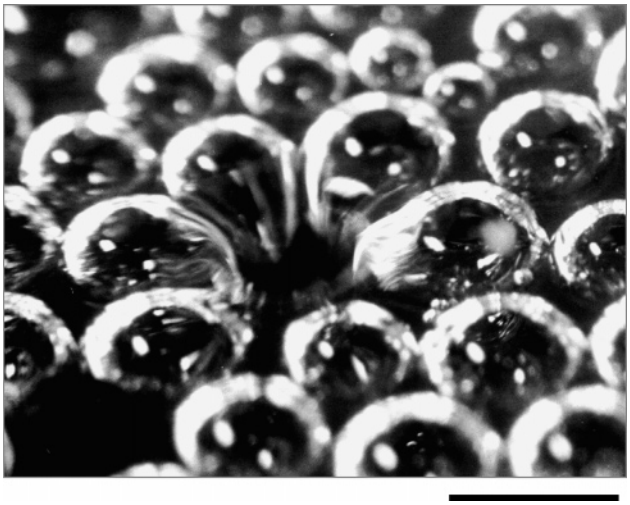

Figure 22. Oblique view of a bursting event in a bubble raft composed of quite monodisperse millimetric bubbles. Bar = 1 mm.

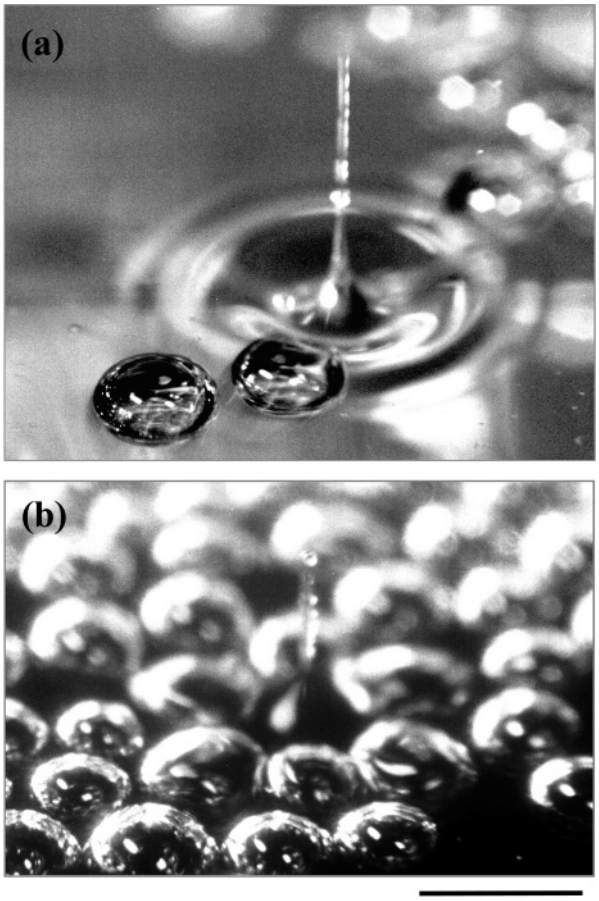

Figure 23. Two oblique views of the liquid jet as it divides into jet drops, after the collapse of a single bubble at the liquid surface (**a**) and after the collapse of a bubble in the bubble raft (**b**). Bar = 1 mm.

collapsing bubble case, or does the roughly hexagonal neighboring bubble pattern around a collapsing cavity strongly modify and even prevent its formation? **Figure 23** compares a liquid jet issued from the collapse of a single Champagne bubble (**Figure 23a**) with a liquid jet issued from a bubble collapsing in a bubble raft (**Figure 23b**). The jet issued from the single collapsing bubble seems to be better "developed" than that issued from the bubble collapsing in the bubble raft. The same tendency has been noted on the very few snapshots that froze the jet in a bubble raft (*63*). Nevertheless, too few snapshots froze this fleeting liquid jet to enable us to make any definite conclusions about similitude and differences with the dynamics of the jet following a single bubble collapse. Further experimental and also numerical investigations are to be conducted along these lines to better understand the role played by the bursting of bubbles in Champagne and sparkling wines.

6. SOME FUTURE PROSPECTS

From the physicochemical point of view, the three phases of a Champagne bubble's life are summarized and illustrated in this review (nucleation, rise, and burst). Nevertheless, some bubbling properties are still not fully understood and therefore need further investigation, especially during the bubble nucleation process.

For example, recently, a surprising and unexpected phenomenon was observed on the wall of a glass poured with Champagne, during the bubbling process. During the gas-discharging process, the clockwork regularity of bubble production from some nucleation sites may sometimes be suddenly broken (*64*). Actually, the close-up observation (conducted in situ from high-speed video camera recordings) revealed an oscillation of the bubble embryo trapped inside the fiber's lumen and also sometimes interactions between numerous embryos inside the lumen of a single fiber. Further investigations are planned to try to model and better understand the bubbling dynamics of some nucleation sites, where numerous gas pockets are interacting. Moreover, Champagne is a very complex liquid matrix. Dissolved salts, carbohydrates, mineral ions, etc., could affect the colligative properties of the test matrix and, thus, the mobility of CO_2 molecules, which could therefore affect in turn the overall kinetics of the bubble nucleation process and growth during ascent. The recent improvements in molecular dynamics simulation studies could maybe help us in better understanding, at the molecular scale, the interactions between the CO_2 molecule and the other species around. Experiments are to be conducted along these lines.

ACKNOWLEDGMENT

Thanks are due to Philippe Jeandet and Bertrand Robillard, for helpful advice and valuable discussions, and to Champagne Moët & Chandon and Pommery for supplying wine samples.

LITERATURE CITED

(1) Liger-Belair, G. *Uncorked: The Science of Champagne*; Princeton University Press: Princeton, NJ, 2004.
(2) Liger-Belair, G. The science of bubbly. *Sci. Am.* **2003**, *288*, 80−85.
(3) Agabaliantz, G. G. Bases scientifiques de la technologie des vins mousseux. *Bull. O. I. V.* **1963**, *36*, 703−714.
(4) Lide, D. R.; Frederikse, H. P. *CRC Handbook of Chemistry and Physics*, 76th ed.; CRC Press: Boston, MA, 1995.
(5) Dussaud, A. Etude des propriétés de surface statiques et dynamiques de solutions alcooliques de protéines: Application à la stabilité des mousses de boissons alcoolisées, Ph.D. Thesis, ENSIAA, Massy, France, 1993.
(6) Lide, D. R. *CRC Handbook of Chemistry and Physics*, 71st ed.; CRC Press: Boston, MA, 1991.
(7) Autret, G.; Liger-Belair, G.; Nuzillard, J.-M.; Parmentier, M.; Dubois de Montreynaud, A.; Jeandet, P.; Doan, B. T.; Beloeil, J.-C. Use of magnetic resonance spectroscopy for the investigation of the CO_2 dissolved in champagne and sparkling wines: A nondestructive and unintrusive method. *Anal. Chim. Acta* **2005**, in press.

(8) Lubetkin, S. D.; Blackwell, M. The nucleation of bubbles in supersaturated solutions. *J. Colloid Interface Sci.* **1988**, *126*, 610−615.
(9) Liger-Belair, G. Physicochemical approach to the effervescence in Champagne wines. *Ann. Phys.* (*Paris*) **2002**, *27* (4), 1−106.
(10) Wilt, P. M. Nucleation rates and bubble stability in water−carbon dioxide solutions. *J. Colloid Interface Sci.* **1986**, *112*, 530−538.
(11) Jones, S. F.; Evans, G. M.; Galvin, K. P. Bubble nucleation from gas cavities: A review. *Adv. Colloid Interface Sci.* **1999**, *80*, 27−50.
(12) Lubetkin, S. D. Why is it much easier to nucleate gas bubbles than theory predicts? *Langmuir* **2003**, *19*, 2575−2587.
(13) Casey, J. A. Bubble size, bubble frequency and rate of gas loss in sparkling wines. *Aust. Grapegrower Winemaker* **1988**, *295*, 19−22.
(14) Bisperink, C. G. J.; Prins, A. Bubble growth in carbonated liquids. *Colloids Surf. A* **1994**, *85*, 237−253.
(15) Liger-Belair, G.; Marchal, R.; Robillard, B.; Vignes-Adler, M.; Maujean, A.; Jeandet, P. Study of effervescence in a glass of champagne: Bubble formation frequencies, growth rates and velocities of rising bubbles. *Am. J. Enol. Vitic.* **1999**, *50*, 317−323.
(16) Carr, M. W.; Hillman, A. R.; Lubetkin, S. D. Nucleation rate dispersion in bubble evolution kinetics *J. Colloid Interface Sci.* **1995**, *169*, 135−142.
(17) Liger-Belair, G.; Vignes-Adler, M.; Voisin, C.; Robillard, B.; Jeandet, P. Kinetics of gas discharging in a glass of champagne: The role of nucleation sites. *Langmuir* **2002**, *18*, 1294−1301.
(18) Liger-Belair, G.; Marchal, R.; Jeandet, P. Close-up on bubble nucleation in a glass of champagne. *Am. J. Enol. Vitic.* **2002**, *53*, 151−153.
(19) Liger-Belair, G.; Topgaard, D.; Voisin, C.; Jeandet, P. Is the wall of a cellulose fiber saturated with liquid whether or not permeable with CO_2 dissolved molecules? Application to bubble nucleation in champagne wines. *Langmuir* **2004**, *20*, 4132−4138.
(20) O'Sullivan, A. Cellulose: The structure slowly unravels. *Cellulose* **1997**, *4*, 173−207.
(21) Liger-Belair, G.; Marchal, R.; Robillard, B.; Dambrouck, T.; Maujean, A.; Vignes-Adler, M.; Jeandet, P. On the velocity of expanding spherical gas bubbles rising in-line in supersaturated hydroalcoholic solutions: Application to bubble trains in carbonated beverages. *Langmuir* **2000**, *16*, 1889−1895.
(22) Liger-Belair, G.; Prost, E.; Parmentier, M.; Jeandet, P.; Nuzillard, J.-M. Diffusion coefficient of CO_2 molecules as determined by ^{13}C NMR in various carbonated beverages. *J. Agric. Food Chem.* **2003**, *51*, 7560−7563.
(23) Einstein, A. Über die von der molekularkinetischen theorie der wärme geforderte bewegung von in ruhenden flüssigkeiten suspendierten teilchen. *Ann. Phys.* (*Leipzig*) **1905**, *17*, 549. Reproduced in *Investigations on the Theory of the Brownian Movement*; Dover Publications: New York, 1956.
(24) Bond, V. N. Bubbles, drops and Stokes' law. *Philos. Mag.* **1927**, *4*, 889−898.
(25) Scriven, L. E.; Sternling, C. V. The Marangoni effects. *Nature* **1960**, *187*, 186−188.
(26) Levich, V. G. *Physicochemical Hydrodynamics*; Prentice Hall: Englewood Cliffs, NJ, 1962.
(27) Davis, R. E.; Acrivos, A. The influence of surfactants on the creeping motion of bubbles. *J. Fluid Mech.* **1966**, *21*, 681−685.
(28) Aybers, N. M.; Tapuccu, A. Studies on the drag and shape of gas bubbles rising through a stagnant liquid. *Waerme- Stoffuebertrag.* **1969**, *2*, 171−177.
(29) Harper, J. F. On bubbles with small immobile adsorbed films rising in liquids at low Reynolds numbers. *J. Fluid Mech.* **1973**, *58*, 539−545.
(30) Rulev, N. N. Hydrodynamics of a rising bubble. *Colloid J.* **1980**, *42*, 210−219.
(31) Duineveld, P. C. Bouncing and coalescence of two bubbles in water. Ph.D. Thesis, University of Twente, The Netherlands, 1994.
(32) Cuenot, B.; Magnaudet, J.; Spennato, B. The effects of slightly soluble surfactants of the flow around a spherical bubble *J. Fluid Mech*. **1997**, *339*, 25−53.
(33) Ybert, C.; di Meglio, J.-M. Ascending air-bubbles in protein solutions. *Eur. Phys. J. B* **1998**, *4*, 313−319.
(34) Liao, Y.; McLaughlin, J. B. Bubble motion in aqueous surfactant solutions. *J. Colloid Interface Sci.* **2000**, *224*, 297−310.
(35) Brissonnet, F.; Maujean, A. Identification of some foam-active compounds in champagne base wines. *Am. J. Enol. Vitic.* **1991**, *42*, 97−102.
(36) Brissonnet, F.; Maujean, A. Characterization of foaming proteins in a Champagne base wine. *Am. J. Enol. Vitic.* **1993**, *44*, 297−301.
(37) Malvy, J. B.; Robillard, B.; Duteurtre, B. Influence of proteins on the foam behavior of champagne wines. *Sci. Aliments* **1994**, *14*, 88−98.
(38) Marchal, R.; Bouquelet, S.; Maujean, A. Purification and partial biochemical characterization of glycoproteins in a champenois Chardonnay wine. *J. Agric. Food Chem.* **1996**, *44*, 1716−1722.
(39) Clift, R.; Grace, J. R.; Weber, M. E. *Bubbles, Drops and Particles*; Academic Press: New York, 1978.
(40) Magnaudet, J.; Rivero, M.; Fabre, J. Accelerated flows past a rigid sphere or a spherical bubble. Part 1. Steady straining flow. *J. Fluid Mech.* **1995**, *284*, 97−135.
(41) Maxworthy, T.; Gnann, C.; Kürten, M.; Durst, F. Experiments on the rise of air bubbles in clean viscous liquids. *J. Fluid Mech.* **1996**, *321*, 421−441.
(42) Liger-Belair, G.; Jeandet, P. More on the surface state of expanding champagne bubbles rising at intermediate Reynolds and high Peclet numbers. *Langmuir* **2003**, *19*, 801−808.
(43) Shafer, N. E.; Zare, R. N. Through a beer glass darkly. *Phys. Today* **1991**, *44*, 48−52.
(44) Ahmed, M.; Dickinson, E. Effect of ethanol on the foaming of aqueous protein solutions. *Colloids Surf.* **1990**, *47*, 353−365.
(45) Dussaud, A.; Han, G. B.; Ter-Minassian-Saraga, L.; Vignes-Adler, M. Surface properties of protein alcoholic solutions: I. Surface tension. *J. Colloid Interface Sci*. **1994**, *167*, 247−255.
(46) Dussaud, A.; Vignes-Adler, M. Surface properties of protein alcoholic solutions: II. Surface dilational rheology. *J. Colloid Interface Sci*. **1994**, *167*, 256−265.
(47) Dussaud, A.; Vignes-Adler, M. Surface properties of protein alcoholic solutions: III. Aging effect. *J. Colloid Interface Sci*. **1994**, *167*, 266−274.
(48) Puff, N.; Cagna, A.; Aguié-Beghin, V.; Douillard, R. Effect of ethanol on the structure and properties of β-casein adsorption layers at the air−buffer interface. *J. Colloid Interface Sci*. **1998**, *208*, 405−414.
(49) Senée, J.; Robillard, B.; Vignes-Adler, M. Films and foams of Champagne wines. *Food Hydrocolloids* **1999**, *13*, 15−26.
(50) Resch, F. J.; Darrozes, J. S.; Afeti G. M. Marine liquid aerosol production from bursting of air bubbles. *J. Geophys. Res*. **1986**, *91*, 1019−1029.
(51) Liger-Belair, G.; Lemaresquier, H.; Robillard, B.; Duteurtre, B.; Jeandet, P. The secrets of fizz in champagne wines: A phenomenological study. *Am. J. Enol. Vitic.* **2001**, *52*, 88−92.
(52) Spiel, D. E. On the birth of jet drops from bubbles bursting on water surfaces. *J. Geophys. Res.* **1995**, *100*, 4995−5006.
(53) Spiel, D. E. More on the births of jet drops from bubbles bursting on seawater surfaces. *J. Geophys. Res.* **1997**, *102*, 5815−5821.
(54) Spiel, D. E. On the birth of film drops from bubbles bursting on seawater surfaces. *J. Geophys. Res*. **1998**, *103*, 24907−24918.
(55) Spiel, D. E. The number and size of jet drops produced by air bubbles bursting on a fresh water surface. *J. Geophys. Res.* **1994**, *99*, 10289−10296.
(56) Woodcock, A. H.; Kientzler, C. F.; Arons, A. B.; Blanchard, D. C. Giant condensation nuclei from bursting bubbles. *Nature* **1953**, *172*, 1144−1145.
(57) MacIntyre, F. Bubbles: A boundary layer " microtome " for micron-thick samples of a liquid surface. *J. Phys. Chem.* **1968**, *72*, 589−592.

(58) Barger, W. R.; Garret, W. D. Surface-active organic material in the marine atmosphere. *J. Geophys. Res.* **1970**, *75*, 4561−4566.
(59) Blanchard, D. C.; Syzdek, L.Mechanism for the water-to-air transfer and concentration of bacteria. *Science* **1970**, *170*, 626−628.
(60) Blanchard, D. C.; Syzdek, L. Concentration of bacteria in jet drops from bursting bubbles. *J. Geophys. Res.* **1972**, *77*, 5087−5099.
(61) Tominaga, T.; Guimbertau, G.; Dubourdieu, D. Role of certain volatile thiols in the bouquet of aged Champagne wines. *J. Agric. Food Chem.* **2003**, *51*, 1016−1020.
(62) Liger-Belair, G.; Robillard, B.; Vignes-Adler, M.; Jeandet, P. Flower-shaped structures around bubbles collapsing in a bubble monolayer. *C. R. Acad. Sci. Paris, Ser. 4* **2001**, *2*, 775−780.
(63) Liger-Belair, G.; Jeandet, P. Capillary-driven flower-shaped structures around bubbles collapsing in a bubble raft at the surface of a liquid of low viscosity. *Langmuir* **2003**, *19*, 5771−5779.
(64) Liger-Belair, G.; Tufaile, A.; Robillard, B.; Jeandet, P.; Sartorelli, J.-C. Period-adding route in sparkling bubbles, in preparation.

Received for review October 20, 2004. Revised manuscript received February 4, 2005. Accepted February 9, 2005. This research was supported by the Europol'Agro institute, by the Conseil Général de la Marne, and by the AROCU.

JF048259E